

Ultrafast, ultrabright, X-ray holography using a uniformly-redundant array

Stefano Marchesini,^{1,2} Sébastien Boutet,^{3,4} Anne E. Sakdinawat,⁵ Michael J. Bogan,¹ Saša Bajt,¹ Anton Barty,¹ Henry N. Chapman,^{1,6} Matthias Frank,¹ Stefan P. Hau-Riege,¹ Abraham Szöke,¹ Congwu Cui,² Malcolm R. Howells,² David A. Shapiro,² John C. H. Spence,⁷ Joshua W. Shaevitz,⁸ Johanna Y. Lee,⁹ Janos Hajdu,^{3,4} and Marvin M. Seibert⁴

¹*Lawrence Livermore National Laboratory, 7000 East Ave., Livermore, CA 94550, USA.*

²*Advanced Light Source, Lawrence Berkeley National Laboratory, 1 Cyclotron rd. Berkeley, CA 94720, USA**

³*Stanford Synchrotron Radiation Laboratory, Stanford Linear Accelerator Center, 2575 Sand Hill Road, Menlo Park, California 94025, USA.*

⁴*Laboratory of Molecular Biophysics, Department of Cell and Molecular Biology, Uppsala University, Husargatan 3, Box 596, SE-75124 Uppsala, Sweden.*

⁵*Center for X-ray Optics, Lawrence Berkeley National Laboratory, Berkeley, California 94720, USA.*

⁶*Centre for Free-Electron Laser Science U. Hamburg, DESY, Notkestraße 85, Hamburg, Germany.*

⁷*Department of Physics and Astronomy, Arizona State University, Tempe, AZ 85287-1504, USA*

⁸*Department of Physics and Lewis-Sigler Institute, 150 Carl Icahn Laboratory, Princeton, New Jersey 08544, USA.*

⁹*Department of Plant and Microbial Biology, University of California, Berkeley, 648 Stanley Hall 3220, Berkeley, California 94720, USA.*

(Dated: August 12, 2021)

Advances in the development of free-electron lasers offer the realistic prospect of high-resolution imaging to study the nanoworld on the time-scale of atomic motions. We identify X-ray Fourier Transform holography^{1,2,3}, (FTH) as a promising but, so far, inefficient scheme to do this. We show that a uniformly redundant array⁴ (URA) placed next to the sample, multiplies the efficiency of X-ray FTH by more than one thousand (approaching that of a perfect lens) and provides holographic images with both amplitude- and phase-contrast information. The experiments reported here demonstrate this concept by imaging a nano-fabricated object at a synchrotron source, and a bacterial cell at a soft X-ray free-electron-laser, where illumination by a single 15 fs pulse was successfully used in producing the holographic image. We expect with upcoming hard X-ray lasers to achieve considerably higher spatial resolution and to obtain ultrafast movies of excited states of matter.

The ideal microscope for the life and physical sciences should deliver high-spatial-resolution high-speed snapshots possibly with spectral, chemical and magnetic sensitivity. X-rays can provide a large penetration depth, fast time resolution, and strong absorption contrast across elemental absorption edges. The geometry of Fourier transform holography is particularly suited to X-ray imaging as the resolution is determined by the scattering angle, as in crystallography. The problem with conventional Fourier holography is an unfavourable trade off between intensity and resolution. We show here how recent technical developments in lensless flash photography can be used to reduce this effect.

Around the 16th century, European painters used the camera obscura, a dark camera with a pinhole to form an image on a canvas. Even earlier, pinhole cameras had been used to image solar eclipses by Chinese, Arab and European scientists. Scientists and painters knew that a small pinhole was required for reaching high resolution, but the small pinhole also dimmed the light and the image⁵. It was eventually discovered that lenses could collect a larger amount of light without degrading resolution. Shutters and stroboscopic flash illumination allowed recording of the time evolution of the image. The development of the computer allowed a resur-

gence of pinhole techniques and random arrays of pinholes were used, initially in X-ray astronomy^{6,7}. Each bright point of a scene deposits a shadow-image of the pinhole array on the viewing screen. Depth information about the object is encoded in the scaling of the shadow image of the object points⁸. Knowledge of the geometry of the pinhole array (the “coded aperture”) allowed numerical recovery of the image. Eventually the pinholes were replaced by binary URAs which were shown to be optimal for imaging⁴. Their multitudes of sharp features contain equal amounts of all possible spatial frequencies, thereby allowing high spatial resolution without sacrifice of image brightness. URA coded apertures are now commonly used in hard X-ray astronomy⁹, medical imaging¹⁰, plasma research¹¹, homeland security¹² and spectroscopy¹³ to improve brightness where lenses are not applicable.

The forerunner of our x-ray holography with a URA reference source is conventional visible-light FTH¹. The interference pattern between light scattered by an object and light from a nearby pinhole is recorded far downstream (Fig. 1). When this recording (the hologram) is re-illuminated by the pinhole reference wave, the hologram diffracts the wavefront so as to produce an image of the object. A second inverted (“twin”) copy of the

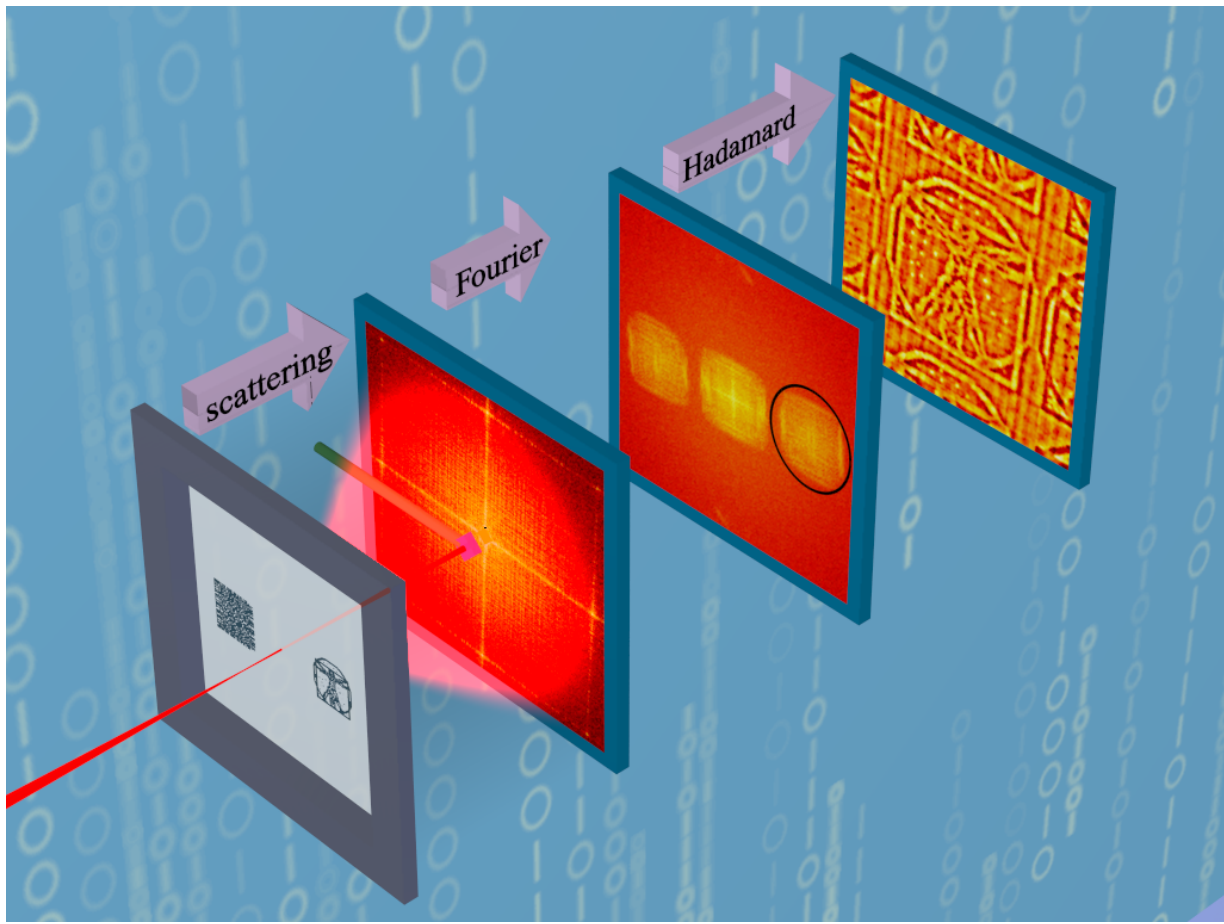


FIG. 1: **Experimental geometry and imaging.** A coherent X-ray beam illuminates both the sample and the Uniformly Redundant Array placed next to it. An area detector (a Charge Coupled Device in these experiments) collects the diffracted X-rays. The Fourier transform of the diffraction pattern yields the autocorrelation map with a holographic term (in the circle) displaced from the center. The Hadamard transform decodes the hologram.

object is produced on the opposite side of the optical axis. Under far-field measurement conditions, a simple inverse-Fourier transform of the FTH recording produces an image of the specimen convolved with the reference pinhole source. As in the pinhole image of the camera obscura, the brightness of the image (or equivalently, the signal to noise ratio) increases as the reference pinhole increases in size, at the expense of image resolution.

In general the solution to the problem of weak signal from a single pinhole (and resulting long exposure time) is to use multiple reference sources. For example, a unique mesoscale object has been imaged by x-ray FTH using 5 pinholes sources¹⁴. No two pairs of pinholes were the same distance apart, so that each holographic term could be isolated in the autocorrelation map. This geometry blocks much of the available light and limits the number of pixels available to image the specimen. Hitherto efforts to produce strong signal have been pursued using complicated reference objects^{1,15,16}. The possible improvement in signal to noise of Fourier-transform holograms with a strong reference saturates¹⁷ at 50% of that for an ideal lens-based amplitude image with loss of phase

information. However there is still the difficulty of deconvolution due to the missing frequency content of the reference. The flat power spectrum of the URA is designed to optimize the reference to fill the detector with light uniformly. In summary, the optimum method of boosting the holographic signal is to use a URA as the reference object. The gain in flux compared to a single pinhole is the number of the opaque elements in the URA (twice as much for phase URAs), in our case, $n=2592$ and $n=162$. The signal to noise ratio (snr) of the URA-produced image increases initially with the square root of the number of pixels in the URA¹³ (see methods), in our case by a factor of 18 and 4.5 for $n=2592$ and $n=162$ respectively.

The x-ray FTH experiment is conceptually simple: a coherent beam of X-rays impinges on a specimen and the coded array, and the diffraction pattern is recorded far downstream (Fig 1). We report here two experiments both using an area detector fitted to an existing experimental end station^{18,20}, and already used in several recent coherent X-ray diffractive imaging experiments^{20,21,22}. The first experiment was carried out at beam line 9.0.1 at the Advanced Light Source (ALS)

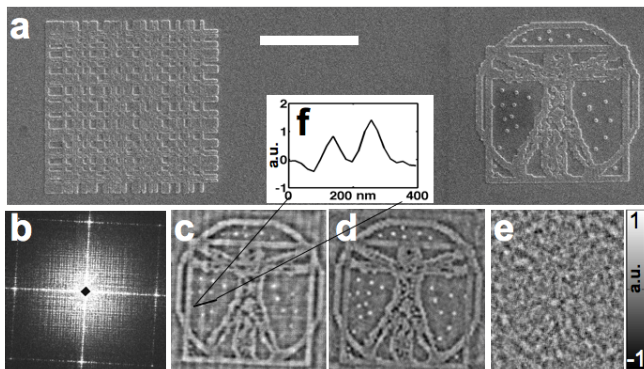


FIG. 2: High resolution holography. (a) Lithographic test sample next to a 10 nm thick twin-prime 71×73 array of 43.5 nm square gold scattering elements, imaged by Scanning Electron Microscopy. Scale bar is $2 \mu\text{m}$. (b) Diffraction pattern collected at the Advanced Light Source ($\lambda=2.3 \text{ nm}$, 10^6 photons in 5 s exposure, 200 mm from the sample). (c) Real part of the reconstructed hologram (linear grayscale), the smallest features of the sample of 43.5 nm are clearly visible. (d) simulation with 10^6 photons. (e) simulation with the same number of photons, but a single reference pinhole. (f) Cut through two dots separated by 120 nm.

at the Lawrence Berkeley National Laboratory. An x-ray beam defined using a $4 \mu\text{m}$ coherence-selecting pinhole was used to image a test object placed next to a 44 nm resolution array (Figure 2). The flux advantage of the URA method is illustrated by the calculations shown in Figs. 2 (c) and (f) and explained in the caption is made evident from our results.

The second series of experiments was carried out at the FLASH soft X-ray free electron laser ($\lambda=13.5 \text{ nm}$) in Hamburg. A 15 fs pulse of 10^{12} photons traverses the sample and URA, and is diffracted just before they both turn into a hot plasma^{20,23}, and become vapourised. A bacterium was imaged to demonstrate that the experiment was feasible with the lower scattering strength of biological material (Fig. 3). More information on these experiments is given in the figure captions and methods section.

In FTH, the final image is produced by an especially simple one-step calculation. A Fourier transformation of the measured intensity pattern delivers the autocorrelation of the wavefield that exits the object plane. In standard FTH with a point reference source such an autocorrelation would already contain the image. For FTH with a URA reference source, it includes the convolution of the object and the URA. Positioning the sample and the array with a sufficient spacing between them ensures that this information-containing term will be separated from the autocorrelations of the array and the object. To extract the final image, we convolved the holographic term (with the rest of the autocorrelation map set to zero) using a mosaic of 3×3 URAs, that is using the same delta-Hadamard transform used to reconstruct the pinhole camera image intensities, but replacing the in-

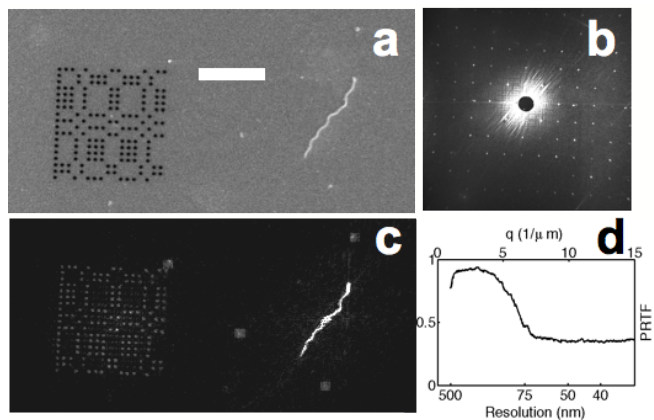


FIG. 3: Ultrafast imaging and phase extension. (a) A URA of pinholes is placed near a Spiroplasma cell (scale bar is $4 \mu\text{m}$). (b) Diffraction pattern collected at FLASH in a single 15 fs ($\lambda=13.5 \text{ nm}$) pulse. (c) Reconstructed image by phase retrieval methods^{26,27}. (d) the reproducibility of the recovered image as a function of spatial frequency drops at 75 nm resolution.

tensity image with the complex valued cross correlation term. The reconstructed images made by this method are shown in Figure 2 using 44-nm URA elements. The forward or small angle scattering was discarded during data collection, yielding edge enhancement in the image. For the biological image additional refinement was demonstrated. By using the Fourier-Hadamard-transform image provided by a 150 nm resolution URA as the starting point for a phase retrieval algorithm, we refined the 15-fs flash image of a small helical bacterium (*Spiroplasma melliferum*) to the full extent of the recorded diffraction pattern at half the pinhole-size resolution (75 nm) (Fig. 3 and methods section).

The resolution of the holograms corresponds to the resolution of the fabricated URAs: 44 nm for the lithographic pattern used at ALS, and 150 nm (refined to 75 nm) for the bacterium used at FLASH. These values are among the best ever reported for holography of a one-micron-sized object, and we believe resolution will improve in the future with the development of nano-arrays. URAs with 25 nm resolution and 9522 elements have already been produced by conventional methods.

In conclusion, we have successfully demonstrated holographic X-ray imaging with URAs and obtained amplified X-ray holographic images at attractive resolutions. These images were orders of magnitude more intense than those from conventional Fourier transform holography, enabling the potential use of novel tabletop sources²⁵. Since URA diffraction uniformly filled the detector with light, image reconstruction could be performed by a Fourier-Hadamard transform in a single step without iterations. The technique shows good prospects for improvements in the spatial resolution, and the results verify the predicted high performance values with respect to high brightness and ultrafast time resolution. Imaging

with coherent X-rays will be a key technique for developing nanoscience and nanotechnology, and or massively parallel holography will be an enabling tool in this quest.

Acknowledgments

We are grateful to the staff of FLASH and ALS for help, and to D. A. Fletcher for the Spiroplasma samples. This work was supported by the following agencies: the U.S. Department of Energy by Lawrence Livermore National Laboratory under Contract W-7405-Eng-48 and DE-AC52-07NA27344; the Advanced Light Source; National Center for Electron Microscopy; Center for X-ray Optics at Lawrence Berkeley Laboratory under DOE Contract DE-AC02-05CH11231; the Stanford Linear Accelerator Center under DOE contract DE-AC02-76-SF00515; the European Union (TUIXS); The Swedish Research Councils, the DFG-Cluster of Excellence through the Munich-Centre for Advanced Photonics; the Natural Sciences and Engineering Research Council of Canada to M. B., and the Sven and Lilly Lawskis Foundation of Sweden to M.M.S.

Methods

Samples. Both ALS and FLASH experiments used samples microfabricated on silicon nitride membranes supported in a silicon window frame. The URA and test pattern for the ALS experiments were fabricated using Center for X-ray Optics nanowriter, Lawrence Berkeley National Lab. Polymethyl methacrylate, a positive resist, was patterned on Si_3N_4 membrane substrate and subsequently gold electroplated (10 nm Au). Patterning dose was achieved in a fraction of a second, enabling potential mass production.

Following glutaraldehyde fixation, Spiroplasma cells were air dried from a solution containing *S. melliferum* on a Si_3N_4 window covered by a 10 nm poly-l-lysine. The URA was fabricated next to a Spiroplasma cell using focused ion beam milling at the National Center for Electron Microscopy.

Data. At the ALS, diffraction patterns were collected using a coherent portion of a soft x-ray beam ($\lambda=2.3$ nm) from an undulator source selected by a $5 \mu\text{m}$ pinhole. The hologram was collected with an in-vacuum back illuminated CCD (1300X1340 $20 \mu\text{m}$ pixels) placed at 200.5 mm from the specimen. The direct beam is blocked by a

beamstop placed in front of the detector to prevent damage to the camera. The beamstop is moved during data collection to recover a large portion of the diffraction pattern. Total collection time was 5 seconds. At FLASH the same CCD is placed at 54.9. mm from the specimen and collects elastically scattered X-rays filtered by a graded multilayer mirror. A hole in the mirror allows the direct beam through, removing the need for a beamstop.

Reconstruction. The autocorrelation map, obtained by Fourier transform of the diffraction pattern, was multiplied by a binary mask 0 in the region outside the cross correlation between the object and the URA (the hologram).). The reconstruction was performed by applying the same processing used for pinhole camera images, by replacing the recorded intensity image with the masked complex valued cross correlation term. A cyclical convolution with a URA decodes the hologram. The URA autocorrelation is a delta function in periodic or cyclical systems, not when surrounded by empty space. To mimic the cyclical correlation, a mosaic of 3X3 binary URAs is convolved with the holographic cross term. The reconstruction procedure retrieves the hologram of the object to a resolution determined by the size the URA elements (at sub-array spacing resolution). However when the spacing between dots is larger than the dots, the array no longer scatters optimally the available light, decreasing the SNR. The signal is proportional to the number of elements in the array, and the noise is proportional to the square root of the number of elements used to deconvolve the image. Only 2X2 URAs contribute to the reconstructed image since the holographic term is at most twice the size as the array itself (the object is smaller than the array). The mosaic URAs are made of +1 and -1 (instead of 1 and 0) terms, yielding an additional factor of $\sqrt{2}$ the noise. The signal to noise ratio therefore increases as $snr_n = snr_1 \frac{\sqrt{n}}{2\sqrt{2}}$. For a phase URA the signal to noise ratio would increase by a factor of 2.

Phase retrieval. The reference points in the URA and a few dust particles were fixed in space throughout the optimization process, facilitating phase retrieval optimization²⁶. The addition of a redundant linear constraint yields more reliable reconstructions, de facto increasing the resolution of the retrieved complex valued images. The rest of the illuminated sample was reconstructed with dynamic support²⁷. The reproducibility of the image as a function of spatial frequency²² drops at 75 nm resolution.

* Correspondance should be addressed to: smarchesini@lbl.gov

¹ Stroke, G. W. *Introduction To Coherent Optics And Holography*, (Academic Press, New York, NY 1969).

² McNulty, I. et al. High-Resolution Imaging by Fourier

Transform X-ray Holography. *Science* **256**, 1009-1012 (1992).

³ Eisebitt, S. et al. Lensless imaging of magnetic nanostructures by X-ray spectro-holography. *Nature* **432**, 885-888 (2004).

- ⁴ Fenimore, E. E. Cannon, T. M. Coded aperture imaging with uniformly redundant arrays. *Appl. Opt.* **17**, 337-347 (1978).
- ⁵ Hammond, J.H. *The Camera Obscura: A Chronicle* (Adam Hilger, Bristol, UK, 1981).
- ⁶ Dicke, R. H. Scatter-Hole Cameras for X-Rays and Gamma Rays. *Astrophys. J.* **153**, L101-106 (1968).
- ⁷ Ables, J. G. Fourier Transform Photography: A New Method For X-Ray Astronomy. *Proc. Astron. Soc. Aust.* **4**, 172-3 (1968).
- ⁸ Nugent, K. A. Chapman, H. N. Kato, Y. Incoherent Soft X-ray Holography. *J. Mod. Opt.* **38**, 1957-1971 (1991).
- ⁹ Caroli, E. Stephen, J. B. di Cocco, G. Natalucci, L. Spizzichino, A. Coded aperture imaging in X- and gamma-ray astronomy. *Space Science Reviews* **45**, 349-403 (1987).
- ¹⁰ Swindell, W. Barrett, H. H. (Editor), *Radiological Imaging: The Theory of Image Formation, Detection, and Processing*. (Academic Press, New York, NY, 1996).
- ¹¹ Fenimore, E. E. Cannon, T. M. Van Hulsteyn, D. B. Lee, P. Uniformly redundant array imaging of laser driven compressions: preliminary results. *Appl. Opt.* **18**, 945-947 (1979).
- ¹² Cunningham, M. et al. First-generation hybrid compact Compton imager. *IEEE Nucl. Sci. Symposium Conference Record* **1**, 312- 315 (2005) .
- ¹³ Harwit, M. Sloane, N.J.A. *Hadamard Transform Optics*, (Academic Press, New York, NY 1979).
- ¹⁴ Schlotter, W. et al. Multiple reference Fourier transform holography with soft x-rays. *Appl. Phys. Lett.* **89**, 163112, (2006).
- ¹⁵ Szöke, A. Holographic Microscopy with a Complicated Reference. *J. Image. Sci. Technol.* **41**, 332-341 (1997).
- ¹⁶ He, H. et al. Use of extended and prepared reference objects in experimental Fourier transform X-ray holography. *Appl. Phys. Lett.* **85**, 2454-2456 (2004).
- ¹⁷ Collier, R. Burkhardt, C. Lin, L. *Optical Holography*. (Academic press, New York, NY, 1971).
- ¹⁸ Beetz, T. et al. Apparatus for X-ray diffraction microscopy and tomography of cryo specimens. *Nucl. Instr. Meth. Phys. Res. A* **545**, 459-468 (2005).
- ¹⁹ Bajt, S Chapman, H. N. Spiller, E. A. Alameda, J. B. Woods, B. W. Frank, M. Bogan M. J., Barty A., Boutet S., Marchesini S, Hau-Riege S. P., Hajdu J., Shapiro D. A camera for coherent diffractive imaging and holography with a soft-X-ray free electron laser, *Appl. Opt.* in press.
- ²⁰ Chapman, H. N. et al., Femtosecond Diffractive Imaging with a Soft-X-ray Free-Electron Laser. *Nature Phys.* **2**, 839-843 (2006), [arXiv:physics/0610044].
- ²¹ Chapman, H. N. et al., High-resolution ab initio three-dimensional X-ray diffraction microscopy. *J. Opt. Soc. Am. A* **23**, 1179-1200 (2006), [arXiv:physics/0509066].
- ²² Shapiro, D. et al. Biological imaging by soft x-ray diffraction microscopy. *Proc. Nat. Acc. Sci. U.S.A.* **102**, 15343-15346 (2005).
- ²³ Chapman, H. N. et al. Femtosecond time-delay X-ray holography. *Nature* **448**, 676-679 (2007).
- ²⁴ Fenimore, E. E. Weston, G. S. Fast delta Hadamard transform. *Appl. Opt.* **20**, 3058-67 (1981).
- ²⁵ Wang, Y. Granados, E. Pedaci, F. Alessi, D. Luther, B. Berrill, M. Rocca, J. J. Phase-coherent, injection-seeded, table-top soft-X-ray lasers at 18.9 nm and 13.9 nm *Nature Photonics* (20 Jan 2008).
- ²⁶ Marchesini, S. A unified evaluation of iterative projection algorithms for phase retrieval. *Rev. Sci. Instr.* **78**, 011301 (2007), [arXiv:physics/0603201].
- ²⁷ Marchesini, S. et al. X-ray image reconstruction from a diffraction pattern alone. *Phys. Rev. B* **68**, 140101(R) (2003), [arXiv:physics/0306174].